Low-temperature superstructure and charge-ordering effect in η-Na1.286V2O5

F. Duc, P. Millet, S. Ravy, A. Thiollet, F. Chabre, A.M. Ghorayeb, F. Mila, A. Stepanov

Low-temperature superstructure and charge-ordering effect in η-$Na_{1.286}V_2O_5$

F. Duc* and P. Millet
Centre d'Elaboration de Matériaux et d'Etudes Structurales, UPR 8011, B.P. 94347, 29 rue Jeanne Marvig, 31055 Toulouse Cedex 4, France

S. Ravy and A. Thiollet
Laboratoire de Physique des Solides, CNRS UMR 8502, Bât. 510, Université Paris-sud, 91405 Orsay Cedex, France

F. Chabre and A. M. Ghorayeb
Laboratoire Matériaux et Microélectronique de Provence, CNRS UMR 6137, Case 142, 13397 Marseille Cedex 20, France

F. Mila
Institut de Physique Théorique, BSP, Université de Lausanne, CH-1015 Lausanne, Switzerland

A. Stepanov
Laboratoire Matériaux et Microélectronique de Provence, CNRS UMR 6137, Case 151, 13397 Marseille Cedex 20, France

(Received 17 May 2003; revised manuscript received 23 September 2003; published 3 March 2004)

In this work, we report on x-ray diffraction, electron spin resonance, and magnetic susceptibility measurements performed on η-$Na_{1.286}V_2O_5$. The x-ray data clearly reveal the existence, around 100 K, of a structural second-order phase transition, stabilizing a superstructure associated with charge ordering. The complete superstructure is determined from x-ray scattering data measured at 15 and 40 K. The low-temperature structure remains centrosymmetric with space group $P2/c$ but with a doubled b lattice parameter. An analysis using superspace symmetry shows that one of the vanadium atoms and its apical oxygen, namely the V7 and O7 atoms, are the most displaced. Two sites for V7 atoms are identified below the transition instead of one with the formal valence of $V^{4.5+}$. We show that these two sites are occupied by V^{4+} and V^{5+}, which corresponds to a charge ordering. We suggest that this transition is driven by electronic repulsions. The magnetic measurements give additional evidence for this transition and for the opening of a spin gap at low temperature. This is discussed in conjunction with superstructure formation.

DOI: 10.1103/PhysRevB.69.094102 PACS number(s): 61.10.−i, 76.30.−v, 71.27.+a

I. INTRODUCTION

Quantum magnetism is nowadays a fashionable topic in the physics of condensed matter. This is related to the exotic magnetic properties observed in low-dimensional quantum spin systems. Initially, most of the studies were dealing with Cu^{2+}-based materials owing to the structural and electronic relationships with high-T_c superconducting layered cuprates.[1–3] Recently however, interest moved to V^{4+} and Ti^{3+}, both ions with a $3d^1$ configuration ($S=\frac{1}{2}$).[4,5] In this context, the sodium-vanadium-oxygen phase diagram has been the subject of intense research. The most striking example is the quarter-filled ladder system[6] α'-NaV_2O_5. Interest in this phase arose not only from the fact that this compound presents a low-temperature spin-gapped phase at $T=34$ K (Ref. 4) but especially from the appearance of a concomitant charge ordering effect—all the vanadium ions are in the valence state +4.5 at high temperature,[6,7] whereas there is evidence for three different valences +4, +4.5, +5 from x-ray scattering experiments[8] at low temperature. If a controversy remained for a while on the nature of the charge ordering (partial or total depending on experiments),[7,8] anomalous x-ray diffraction experiments[9] and *ab initio* calculations[10] have given a clue, indicating that the total charge ordering occurring on the modulated rungs is actually small: $2\delta_{tot}=0.05e^-$.

Recently, the detailed study of the zone of the diagram richer in vanadium V^{4+} has led to the structural characterization of the vanadium oxide bronze η-$Na_{1.286}V_2O_5$.[11,12] This phase, which can also be denoted by the stoichiometric formula $Na_9V_{14}O_{35}$, crystallizes at room temperature in the monoclinic system (space group $P2/c$) with an original structure built up of layers consisting of VO_5 square pyramids sharing edges and corners, with their apical oxygens pointing up and down alternately to form double strings in the [100] direction (Fig. 1). These double strings are isolated in the [001] direction via VO_4 tetrahedra. A peculiar point for $Na_9V_{14}O_{35}$ is that the double strings have a stairlike shape with a step every ten VO_5 square pyramids. The Na atoms are distributed between the layers. It is worth noting that these layers contain V^{4+}, $V^{4.5+}$, and V^{5+} ions.

The magnetic susceptibility of $Na_9V_{14}O_{35}$ was reported to exhibit a spin gap behavior,[12] whereas its crystal structure was quite different from any structure of low-dimensional spin-gap systems, namely, a spin-ladder system, a dimer system, or an alternate chain system. As its susceptibility curve could not be fitted[12] by theoretical equations for spin-gap systems, $Na_9V_{14}O_{35}$ was considered as a new type of low-dimensional systems. A tentative explanation for this spin-gap behavior was then proposed by Whangbo and Koo.[13] The spin-dimer analysis of $Na_9V_{14}O_{35}$ led them to the conclusion that the $V_{10}O_{30}$ chains of this compound are topo-

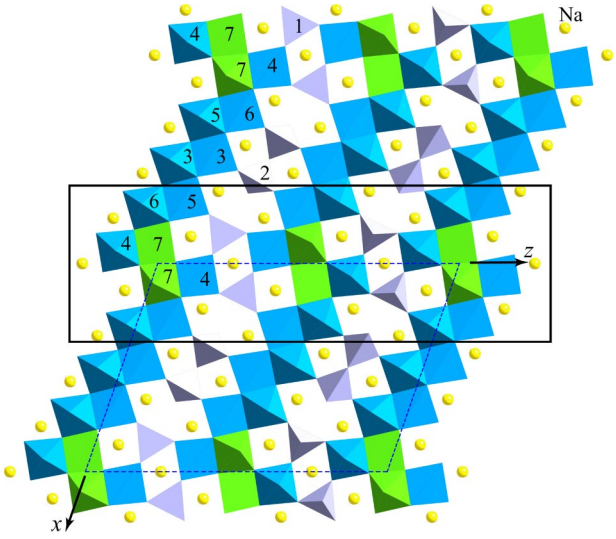

FIG. 1. (Color online) Projection of the $T=300$ K $Na_9V_{14}O_{35}$ structure onto (010) (polyhedra representation). The numbers 1–7 represent the nonequivalent vanadium atoms Vi ($i=1-7$). The V1 and V2 (V^{5+}) atoms are in a tetrahedral coordination, the Vi ($i=3-6$,V^{4+}) are in square pyramids of O atoms. The V7 ($V^{4.5+}$) are in smaller square pyramids.

logically equivalent to a fused chain of 10-node rings. However, we believe on general grounds that this cannot be the case, as discussed in the last section. In addition, this explanation does not take into account the anomalous kink observed around 100 K in the susceptibility curve.[12,14] In order to understand this anomalous behavior, we have undertaken single-crystal x-ray diffraction experiments at low-temperature combined with complementary magnetic susceptibility and electron spin resonance (ESR) measurements.

II. EXPERIMENTAL SECTION

A. Synthesis: Crystal growth

Single crystals of $Na_9V_{14}O_{35}$ were synthesized in two steps: first, powder samples were prepared in a gold crucible by a solid-state reaction as follows. A stoichiometric mixture of V_2O_3, V_2O_5, and $NaVO_3$ was ground in an agate mortar and then annealed in a vacuum-sealed quartz tube at 620 °C for 12 h. In a second step, single crystals were grown from the melt by maintaining the powder for 6 h at 700 °C, and then following this by a slow cooling down to 650 °C at a rate of 2 °C/h.

B. Magnetic measurements

As far as the magnetic measurements are concerned, the susceptibility of $Na_9V_{14}O_{35}$ samples was measured as a function of temperature, between 1.8 and 330 K, in a field of 1 T, using a Quantum Design SQUID magnetometer. In addition, single crystals were studied by ESR spectroscopy between 4.2 and 300 K, using a Bruker EMX spectrometer operating in the X band ($\nu=9.635$ GHz).

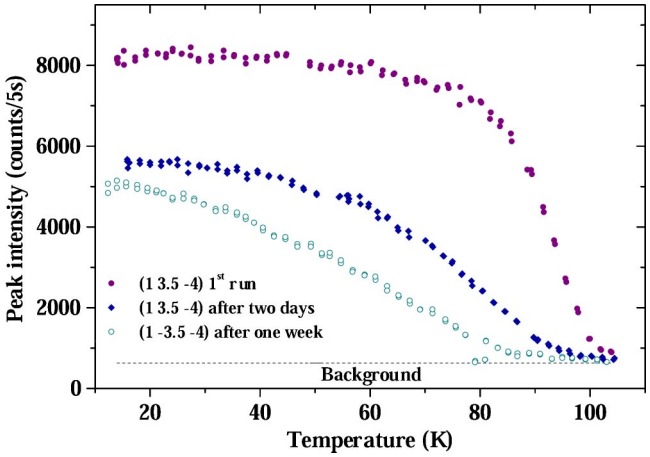

FIG. 2. (Color online) Peak intensity of the symmetry equivalent (1 3.5 $\bar{4}$) (full symbols) and (1 $\bar{3.5}$ $\bar{4}$) (open circles) superstructure reflections as a function of temperature, at the beginning of the experiment (circles), two days (diamond), and one week (open circles) later.

C. X-ray diffraction

Preliminary x-ray diffraction experiments were first carried out with the so-called fixed-film–fixed-crystal method in order to detect a structural change. Accurate measurements were then performed using a three-circle diffractometer. Monochromatic x rays ($\lambda=1.5418$ Å) Cu $K\alpha$ were obtained from either a classical tube or from a rotating anode (12 kW generator). The setups were equipped with closed-cycle helium cryostats operating from 300 K down to 15 K. A single crystal of size $1\times0.8\times0.1$ mm^3 was studied.

The photographic study showed the appearance below $T_c=100$ K of superstructure reflections at the reduced wave vector $\mathbf{q}_c=(0,\frac{1}{2},0)$, indicating the occurrence of a structural phase transition resulting in the doubling of the unit cell in the **b** direction. The diffractometric study confirmed this first result. The superstructure spots were found to have the same half width at half maximum (HWHM) as that for the main Bragg reflections (1.69, 0.22, and 0.26 nm^{-1} in the **a***, **b***, and **c*** directions, respectively), indicating the stabilization of a long-range order below T_c. Figure 2 shows the peak intensity of the (1 3.5 $\bar{4}$) and (1 $\bar{3.5}$ $\bar{4}$) superstructure reflections as a function of temperature. These curves gradually changed during the experiment. At the beginning of the experiment, the structural phase transition was observed at T_c, as evidenced by the continuous increase of the intensity below T_c typical of a second-order phase transition.[15] Two days or one week later, a gradual decrease of the low-temperature intensity was observed. A possible origin for this phenomenon could be an effect of irradiation, although this is rarely observed in inorganic systems in such experimental conditions. Another possibility could also be a stress effect since, in our experiment, the sample was fixed with silver dag and hence was not free to move while undergoing its structural phase transition.

This second-order transition is announced by a sizable regime of fluctuations, as evidenced by the presence of broad diffuse scattering around the q_c wave vector above T_c. Fig-

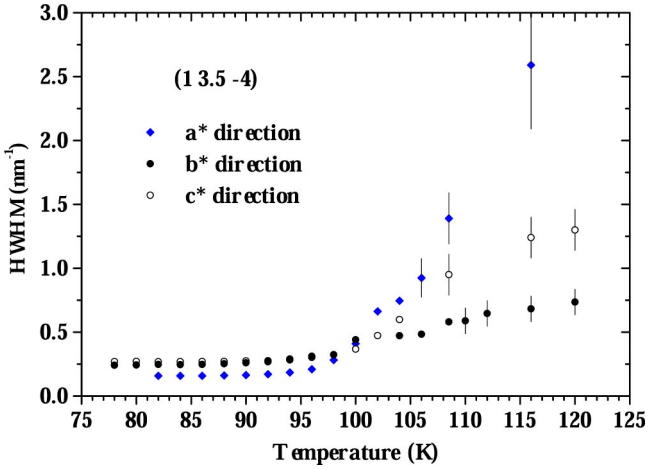

FIG. 3. (Color online) Half width at half maximum of the (1 3.5 $\bar{4}$) scattering in the **a*** (diamond), **b*** (full circle), and **c*** (open circle) directions as a function of temperature.

ure 3 displays the temperature dependence of the HWHMs around the (1 3.5 $\bar{4}$) reciprocal position. Upon heating, the HWHMs deviate from their low-temperature value at ~100 K, with an increase rate strongly dependent on the direction. In a simple Ginzburg-Landau approach, the correlation lengths of these pretransitional fluctuations are equal to the inverse of the HWHMs, deconvoluted from the instrumental resolution. Figure 3 clearly shows that the correlation lengths along the in-plane directions **a*** and **c*** become smaller than the unit-cell dimensions (1.52 nm and 2.077 nm) only 5–10 K above the transition temperature. At variance, the correlation lengths along the **b*** directions reach 2 nm at 120 K, which is still about $4b$. This shows that this phase transition has a one-dimensional character, and that the driving force of the instability is mainly in the **b** direction. These surprising results called for the refinement of the low-temperature structure of $Na_9V_{14}O_{35}$.

Therefore, single-crystal x-ray measurements were performed at 15 K and 40 K. Since the results are quite similar, in the following only the results at 40 K will be presented (the data at 15 K are given in supplementary material[16]). A needlelike single crystal was mounted on an Xcalibur CCD diffractometer (Oxford Diffraction) using graphite monochromated Mo $K\alpha$ ($\lambda = 0.710\ 73$ Å) radiation. The temperature was controlled using a helium gas cryostream cooler (Helijet Oxford Cryosystems). A crystal-to-detector distance of 60 mm was set for the measurement.

The lattice parameters of the basic-structure unit cell at both temperatures were determined with the standard diffractometer software CRYSALIS RED (Ref. 17) from a peak search over the measured raw images. A monoclinic lattice was found with $a = 15.2006(8)$ Å, $b = 5.0001(3)$ Å, $c = 20.776(1)$ Å, $\beta = 109.128(6)°$ and $a = 15.2008(8)$ Å, $b = 4.9989(3)$ Å, $c = 20.766(1)$ Å, $\beta = 109.118(6)°$ for 15 and 40 K, respectively. As the additional reflections were very weak in comparison with the main reflections, the values of the modulation vector parameters were estimated by analyzing the reconstructed layers.

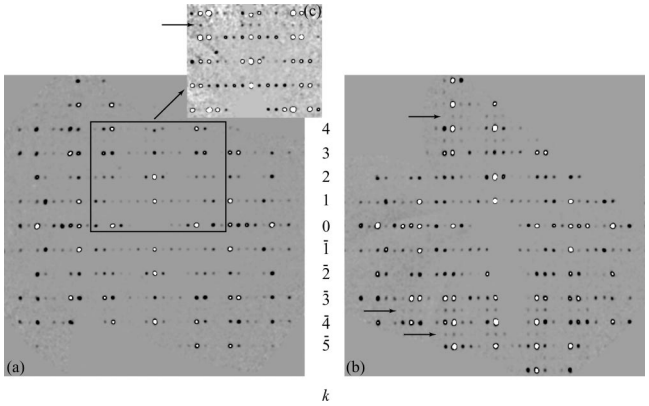

FIG. 4. Reciprocal layer $hk0$ reconstructed from the frames of the data collections using the standard diffractometer software CRYSALIS RED (Ref. 17): (a) at 91 K, (b) at 40 K. The superstructure reflections are marked by arrows. (c) Detail of (a) with gray scale multiplied by 15 to enhance the low-intensity phenomena at 91 K. Holes appear in the reconstructed layers because the data collections did not cover the whole Ewald sphere and because of the blind regions inherent to the collection method. .

A comparison of the $hk0$ layer at $T = 91$ K [preliminary single x-ray diffraction study with a crystal mounted on an Xcalibur CCD diffractometer equipped with a nitrogen gas cryostream cooler (Cryojet Oxford Cryosystems)] and $T = 40$ K is given in Fig. 4. All the reflections observed on the collected frames were indexed with four integers $hklm$ according to the four-dimensional base[18,19] $\mathbf{H} = h\mathbf{a}^* + k\mathbf{b}^* + l\mathbf{c}^* + m\mathbf{q}$ where $\mathbf{a}^*, \mathbf{b}^*, \mathbf{c}^*$ are the reciprocal axes of the basic structure and $\mathbf{q}$ is the modulation vector. The main reflections have $m = 0$. The commensurate values of the modulation vector parameters $(0, \frac{1}{2}, 0)$ were verified with the program NADA.[20] As the structure is commensurately modulated, the diffracted intensities can be interpreted as a projection from the (3+1)-dimensional superspace into three-dimensional physical space and then indexed by four integers $hklm$, as well as a classical three-dimensional diffraction pattern and then be indexed by three integers hkl. Both approaches were performed but the superspace description of the structure was finally preferred. Indeed, the use of higher-dimension crystallography has several advantages over the three-dimensional (3D) approach; it allows (i) a unique description of the various existing phases of crystals undergoing phase transitions and (ii) in some cases, usually when satellite reflections are very weak and cannot be observed up to high orders, a much better control of the number of refined parameters in terms of the number of modulation waves (in a 3D approach the refinement of the maximum number of parameters would lead to parameter correlations). Whatever the description of a commensurate structure (by modulation functions or in the supercell) they should be equivalent. Therefore the number of refined parameters should be the same in both approaches.[21]

The extraction of intensities from the measured raw images was done with the standard diffractometer software CRYSALIS RED.[17] As a result of integration, the intensities and σ of all reflections $hklm$ were obtained. The integrated intensities were corrected for Lorentz and polarization effects.

TABLE I. Experimental details.

	Temperature (K)	
	15(2)	40(1)
Crystal data		
Chemical formula	$Na_9V_{14}O_{35}$	—
Chemical formula weight (g mol^{-1})	1480	—
Cell setting, superspace group	Monoclinic, $P2/c(0\beta0)00$	—
a, b, c (Å)	15.2006(8), 5.0001(3), 20.776 (1)	15.2008(8), 4.9989(3), 20.766(1)
β (deg)	109.128(6)	109.118(6)
V (Å^3)	1491.9(2)	1490.9(2)
Z	2	—
D_x (Mg m^{-3})	3.29	—
μ (mm^{-1})	4.424	—
Crystal form, color	Needle, metallic dark blue	—
Crystal size (mm)	$0.89\times0.14\times0.118$	—
Modulation vector	$\mathbf{q}=0.502(6)\ \mathbf{b}^*$	$\mathbf{q}=0.499(4)\ \mathbf{b}^*$
Data collection		
Radiation type	Mo $K\alpha$	—
Diffractometer	Xcalibur CCD	—
Data collection method	ω scans	—
Absorption correction	Gaussian	—
T_{min}	0.251	0.245
T_{max}	0.627	0.624
No. of measured, independent and observed reflections	32594, 12847, 5175	32589, 12832, 5126
No. of main reflections	3626	3628
No. of satellite reflections	1549	1498
R_{int}	0.0797	0.0785
θ_{max} (deg)	31.19	31.26
Range of h,k,l,m	$-21\rightarrow21$	—
	$-7\rightarrow7$	—
	$-28\rightarrow29$	—
	$-1\rightarrow1$	—
Refinement		
Refinement on	F	—
Criterion for observed reflections	$I>3\sigma(I)$	—
Weighting scheme	$w=1/[\sigma^2(F)+0.0049F^2]$	—
Extinction correction	Becker and Coppens[a] type 1 Gaussian isotropic	—
Extinction coefficient	0.24 (4)	0.22 (4)
R, wR, S (all reflections)	0.0451, 0.0996, 1.21	0.0465, 0.1038, 1.26
R, wR (main reflections)	0.0395, 0.0773	0.0402, 0.0742
R, wR (satellites)	0.1178, 0.1895	0.1333, 0.2053
$(\Delta/\sigma)_{max}$	0.0047	0.0015
$\Delta\rho_{max}$, $\Delta\rho_{min}$ (e Å^{-3})	2.19, −1.79	1.92, −1.86
No. of reflections and parameters used in refinement	5175, 350	5175, 350
Source of atomic scattering factors	[b]	

[a]Reference 34.
[b]Reference 19.

Absorption was corrected analytically using the crystal shape and the indices of the faces determined by the program MOVIE.[17]

The crystal data as well as the conditions for data collection and refinement are summarized in Table I.

III. STRUCTURE DETERMINATION AND REFINEMENT

The systematic extinctions were derived from the reconstructed images of reciprocal-lattice planes such as those shown in Fig. 4. The appearance of main reflections is in

agreement with the space group $P2/c$, and the satellite reflections appear only for those main reflections allowed by this space group. The additional reflections do not introduce other systematic absences and are then in agreement with the extinction rule ($h0l0, l=2n$), which leads to $P2/c(0\beta0)00$ as the superspace group.[19,22] From the magnitude of the satellites one can estimate that the atomic displacements from the room-temperature structure will be small. Consequently, the structure refinement of the basic structure was initiated with the model obtained at room temperature[11] using the program JANA2000.[23] The contribution of the satellite reflections is neglected in this step, only main reflections are used.

These refinements using anisotropic displacement parameters converged to $R(\text{obs/all})=0.0396/0.0446$ and $wR(\text{obs/all})=0.0737/0.0800$ for 3628 reflections. $R(\text{obs})$ refers to reflections with $I>3\sigma(I)$. In total 264 parameters have been refined. The average structure obtained was quite similar to the model determined at room temperature, except for the atomic displacement parameters, which were in accordance with low-temperature measurements. The V atoms at site V7 exhibited, however, the most anisotropic displacement parameters with $U^{22}>5U^{11}$ and $U^{22}>2.5U^{33}$ at both temperatures. It is interesting to note that the vanadium on this site was in the partial oxidation state $V^{4.5+}$ at room temperature. The O atoms at the oxygen apical site O7 showed very anisotropic displacement parameters with $U^{22}>1.75U^{11}$ and $U^{22}>2U^{33}$ as well. This led us to assume that the modulation has basically a displacive character and mainly affects the positions of V7 atoms and of their nearest neighbors along the [010] direction.

This average model was used as a starting point for the refinement of the modulated structure. The modulation was determined by the refinement of all independent modulation amplitudes against the intensities of the main reflections and first-order satellites. The modulation function of a commensurate structure is defined only in points corresponding to N positions of relevant atoms in an N-fold superstructure ($N=2$ in our case). Therefore it can be completely described by a finite Fourier expansion. Because of the commensurateness, we have to find the value of t_0 corresponding to the true structure,[21,24] where t_0 denotes the starting phase of the commensurate modulation function. The correct t_0, defining the symmetry of the superstructure, has to be determined from the refinement. Subsequently, in a trial-and-error process, several models with different symmetry were tried. For each model, we included step by step one wave for a displacive modulation for each atom.

The best solution was obtained with a simple harmonic displacement of all atoms. The value of t_0 yielding the best fit between the observed and calculated structure factors was $\frac{1}{4}$. This means that the modulation functions of each atom can only be interpreted along the internal space[25,26] at $t=\frac{1}{4}$ and $\frac{3}{4}$. The symmetry of the superstructure on the corresponding $a\times 2b\times c$ supercell is then equivalent to that of the $P2/c$ space group, but the translational symmetry of the b lattice spacing, which kept the crystal invariant at room temperature, is no longer a symmetry at low temperature. This structural phase transition is therefore characterized by symmetry breaking, which is typical of a second-order transition.

Because of the missing second-order reflections, it was sufficient to include the first-order harmonics in the refinements. Only the components of the amplitude of the sine term were refined. The final refinement converged to $R=0.0465$ for all observed reflections ($R=0.0402$ for the main and $R=0.1333$ for the satellite reflections). The results of the refinement of the commensurately modulated structure are given in Tables II and III.

IV. RESULTS AND DISCUSSION

A. Structure at low temperature

The main contribution to the intensity of the satellite reflections originates from the deviation of the V atoms at the site V7 from their average position. Among the V atoms, the V7 atom displays by far the largest modulated amplitude. The O7-atom position, which is the apical oxygen site of V7, has larger amplitudes (see Table III), but because of its relatively weak scattering factor, its contribution to the satellite intensity is less. Two Na atoms contribute also to the intensity of the satellite reflections, namely, the Na1 and Na5 sites, which are close to the V7 site. The other atoms remain almost fixed. The modulations mainly occur along the [010] direction, indicating the longitudinal mode of displacements. In terms of superstructure description, the number of atom sites is twice as large (one type of site is given for $t=\frac{1}{4}$ and the other for $t=\frac{3}{4}$). Whereas most of the atoms are not displaced from their average positions, the modulations give rise to two distinct positions along the **b** axis for the atoms V7, O7, Na1, and Na5.

The variations of the distances between the atoms for V-O polyhedra are given for the two commensurate sections $t=\frac{1}{4}$ and $\frac{3}{4}$ (Table IV). The model obtained shows that the V7-O7 bonds remain unchanged with respect to room temperature. This means that V7 and O7 move in phase along the [010] direction. On the other hand, as the other oxygen atoms are almost not displaced from their average position, one can clearly identify two types of V-O basal plane pyramid changes in the first coordination sphere of V7: an expansion (for $t=\frac{1}{4}$) and a contraction (for $t=\frac{3}{4}$). As the formal valence of $V^{4.5+}$ was assigned to the V7 site at room temperature, we attribute the formal valence state V^{4+} to the expanded pyramid containing the first kind of V7 position, and the oxidation state V^{5+} to the contracted pyramid containing the second type of V7 position. This hypothesis was confirmed with the calculation of the valences of V sites as a function of t using the bond-valence method.[27] The results of this analysis are reported in Table V. The alternation of the two kinds of V7 sites along the **b** axis results in a sequence $4+, 5+, 4+, 5+, \ldots$ for the atoms on V7 (Fig. 5). It is worth noting that the V7 atoms move in opposite directions from one plane to another with regard to their position at room temperature. This leads to two types of distances between the apical oxygen O7 and the V7 atoms of the next layer: 3.314(2) Å for V^{4+} to apical O-V^{5+} and 3.550(2) Å for V^{5+} to apical O-V^{4+} at 40 K in comparison with 3.463(2) Å at room temperature.

Moreover, according to the symmetry of the superspace, the centers of symmetry located on (000) and $(0\frac{1}{2}0)$ are lost,

TABLE II. Final values of coordinates and Fourier amplitudes of the displacive modulation functions at $T=40$ K for vanadium and sodium atoms [$U_{eq}=(1/3)\Sigma_i\Sigma_j U^{ij}a^i a^j \mathbf{a}_i\cdot\mathbf{a}_j$; s,1 are components of the sine term, first-order harmonic].

Atom	Wave	x	y	z	U_{eq} (Å^2)
V1		0.14480(3)	0.91803(9)	0.81787(2)	0.00508(16)
	s,1	−0.00113(2)	−0.00032(6)	0.000036(15)	
V2		0.40282(3)	0.85589(10)	0.76873(2)	0.00505(16)
	s,1	−0.00045(2)	−0.00111(6)	−0.000601(16)	
V3		0.48754(3)	0.90038(9)	0.56432(2)	0.00448(18)
	s,1	−0.00015(2)	−0.00149(5)	−0.000076(16)	
V4		0.06343(4)	0.91179(10)	0.65011(3)	0.00454(16)
	s,1	−0.00008(2)	0.00054(6)	−0.000230(15)	
V5		0.69864(3)	0.89702(9)	0.52276(3)	0.00456(17)
	s,1	−0.00021(2)	−0.00056(5)	−0.000240(16)	
V6		0.27545(3)	0.90018(10)	0.60612(3)	0.00465(18)
	s,1	−0.00078(2)	0.00011(5)	−0.001012(16)	
V7		0.90709(3)	0.88108(9)	0.47778(2)	0.00526(15)
	s,1	0.00073(2)	0.01244(6)	0.000638(16)	
Na1		0	0.3982(3)	0.75	0.0079(5)
	s,1	0	0.0127(6)	0	
Na2		0.21803(8)	0.3815(2)	0.70002(6)	0.0079(4)
	s,1	0.00362(13)	−0.0009(4)	0.00391(10)	
Na3		0.43283(9)	0.3723(2)	0.65457(7)	0.0071(4)
	s,1	0.00396(12)	−0.0024(3)	0.00299(9)	
Na4		0.65263(8)	0.3720(2)	0.61771(6)	0.0079(4)
	s,1	0.00292(12)	0.0032(4)	0.00252(9)	
Na5		0.87020(9)	0.3546(2)	0.57851(6)	0.0087(4)
	s,1	−0.00010(11)	0.0158(3)	0.00364(8)	

and only those located on $(0\frac{1}{4}0)$ and $(0\frac{3}{4}0)$ remain, i.e., those that are out of the layers defined by the V polyhedra. The VO_5 square pyramids pointing up and down along a double string in the same layer are therefore no longer equivalent below the transition, whereas they were equivalent 2×2 by symmetry at room temperature. This is particularly relevant for the adjacent pyramids containing the V7 atoms. Indeed, these adjacent pyramids correspond to the two types of pyramids observed above, i.e., the expanded one and the contracted one (Fig. 6). This results in a peculiar charge ordering along the infinite double strings in the (**a**,**c**) planes. Indeed, on the ten VO_5 square pyramids along the double strings in the stairlike shape, nine V cations are in the oxidation state V^{4+} and one, which is located at the corner of the double string, is in the V^{5+} state [Fig. 5(a)]. The distance between V7 atoms of adjacent pyramids remains unchanged [2.9225(8) Å at 40 K compared with 2.9230(9) Å at room temperature].

As mentioned earlier, the modulations are not restricted only to the V7 and O7 atom sites. The Na atoms close to the V7 atoms, i.e., the Na1 and Na5 sites, are also displaced along the [010] direction with respect to their average position. However, their displacements are smaller than those observed for V7 and O7 [$b\triangle y(\mathrm{Na1})\simeq\pm0.075(1)$ Å, $b\triangle y(\mathrm{Na5})\simeq\pm0.150(1)$ Å, $b\triangle y(\mathrm{V7/O7})\simeq\pm0.300(1)$ Å]. Like the V7 atoms along the **b** axis, they move in opposite directions from one layer to another [Fig. 5(b)]. This leads to the alternation of two interlayer distances for each type of these Na sites: 4.970(2) Å and 5.028(2) Å for Na1-Na1, and 4.940(2) Å and 5.059(2) Å for Na5-Na5 at 40 K instead of the unique interplane distance of 5.032(2) Å for Na1-Na1, Na5-Na5 at room temperature. Besides, it is interesting to note that the Na1 and Na5 atoms on both sides of the pyramids containing the V7 atoms in the oxidation state V^{4+} approach V7, whereas those located on both sides of the pyramids containing the V7 atoms in the oxidation state V^{5+} move away from these [Fig. 5(b)]. Two Na1-Na5 distances can be noticed: 3.458(1) and 3.476(1) Å at 40 K instead of 3.459(1) Å at room temperature. The bond lengths for Na-O polyhedra for the two commensurate sections $t=\frac{1}{4}$ and $\frac{3}{4}$ are given in Table VI. According to the most displaced atoms, the largest variations of the distances between the atoms are observed for the Na1-O and Na5-O polyhedra.

These results show that the low-temperature phase of $Na_9V_{14}O_{35}$ is characterized by a three-dimensional ordering of the V^{4+} or V^{5+} atoms on the V7 site, which corresponds to a charge ordering. Moreover, it is noteworthy that the correlation lengths measured by diffuse scattering verify $\xi_b>\xi_c>\xi_a$, which indicates that the local charge ordering is more extended when the V-V distance is small. These facts are consistent with a phase transition driven by Coulomb forces, and reinforces the conclusion that it is a charge-ordering transition in nature.

TABLE III. Final values of coordinates and Fourier amplitudes of the displacive modulation functions at $T=40$ K for oxygen atoms [$U_{eq}=(1/3)\Sigma_i\Sigma_j U^{ij}a^i a^j \mathbf{a}_i\cdot\mathbf{a}_j$; s,1 are components of the sine term, first-order harmonic].

Atom	Wave	x	y	z	U_{eq} (Å^2)
O1		0.14065(15)	0.5890(4)	0.81996(11)	0.0083(6)
	s,1	−0.0067(3)	−0.0004(8)	−0.0005(2)	
O2		0.33496(14)	0.6178(4)	0.78089(10)	0.0080(6)
	s,1	−0.0033(2)	−0.0053(7)	−0.00336(16)	
O3		0.49936(15)	0.5826(4)	0.57956(12)	0.0077(6)
	s,1	−0.0051(3)	−0.0061(9)	−0.0019(2)	
O4		0.06237(15)	0.5890(4)	0.65566(11)	0.0080(6)
	s,1	−0.0043(3)	0.0017(8)	−0.0052(2)	
O5		0.70838(15)	0.5785(4)	0.53444(12)	0.0079(6)
	s,1	−0.0010(3)	−0.0012(9)	−0.0034(2)	
O6		0.28666(15)	0.5821(4)	0.62129(11)	0.0073(6)
	s,1	−0.0078(3)	−0.0049(9)	−0.0080(2)	
O7		0.90235(14)	0.5659(4)	0.48849(11)	0.0086(6)
	s,1	0.0117(4)	0.0532(11)	0.0018(3)	
O8		0.5	0.6875(5)	0.75	0.0065(7)
	s,1	0	−0.0020(5)	0	
O9		0.76352(14)	0.0406(4)	0.61441(10)	0.0072(6)
	s,1	0.00114(8)	0.0003(2)	−0.00007(6)	
O10		0.55343(14)	0.0484(4)	0.65925(10)	0.0072(6)
	s,1	0.00023(8)	0.0002(2)	0.00023(6)	
O11		0.34695(14)	0.0501(4)	0.69898(10)	0.0065(6)
	s,1	0.00012(8)	−0.0017(2)	0.00017(6)	
O12		0.14559(13)	0.0322(4)	0.73900(10)	0.0072(6)
	s,1	0.00042(8)	−0.0038(2)	0.00065(6)	
O13		0.04293(13)	0.0413(4)	0.82775(10)	0.0069(6)
	s,1	−0.00104(8)	0.0034(2)	0.00004(6)	
O14		0.16220(13)	0.0347(4)	0.61653(10)	0.0069(6)
	s,1	0.00018(8)	0.0014(2)	0.00035(6)	
O15		0.37307(14)	0.0335(4)	0.57428(10)	0.0064(6)
	s,1	0.00024(8)	0.0012(2)	0.00011(6)	
O16		0.58470(14)	0.0386(4)	0.53243(10)	0.0062(6)
	s,1	0.00068(8)	−0.0021(2)	0.00050(6)	
O17		0.79828(13)	0.0290(4)	0.49057(10)	0.0062(6)
	s,1	0.00078(7)	0.0001(2)	−0.00046(6)	
O18		0.00871(13)	0.0315(4)	0.94268(10)	0.0068(5)
	s,1	0.00328(8)	−0.0014(2)	0.00050(6)	

B. Magnetic results

In the light of the structural results, we have further examined the magnetic behavior of $Na_9V_{14}O_{35}$. The magnetic susceptibility data of a typical sample of this compound are plotted in Fig. 7. The sample was first cooled down to 1.8 K and then the data were acquired upon heating under a magnetic field of 1 T. The raw data curve, represented by open diamonds and to which we shall refer as χ_{raw}, is similar to what was found by Isobe *et al.*[12] for this compound. χ_{raw} goes through a maximum at about 105 K and shows a small but evident and reproducible kink at 102 K. We associate this feature with the structural and charge ordering transition discussed above. Below this temperature, the susceptibility decreases rapidly down to about 7 K, and then increases at very low temperatures owing to the presence of impurities in the sample. Indeed, we have checked the origin of this low-temperature increase by fitting the low-temperature data points to a Curie-Weiss law, $\chi_{\mathrm{imp}}=p_i C/(T-\theta)$, where p_i would represent the concentration of impurities present. Taking $C=0.365$ cm^3 K mol^{-1} ($S=\frac{1}{2}, g=1.973$), the fitting procedure gives $p_i=0.0053$ and an antiferromagnetic Curie-Weiss temperature $\theta=-3.35$ K. The susceptibility of these impurities, χ_{imp}, is shown as a solid line in Fig. 7. By subtracting χ_{imp} from χ_{raw}, we then obtain the susceptibility, χ, of the pure $Na_9V_{14}O_{35}$ phase, represented in Fig. 7 by open circles. It is clear that this corrected susceptibility goes to zero at very low temperatures, indicating the presence of a spin gap in the system.

TABLE IV. Bond lengths (Å) for V-O polyhedra at 40 K. Symmetry codes: (i) $1-x,1+y,3/2-z$; (ii) $x,1+y,z$; (iii) $1-x,1-y,1-z$; (iv) $-x,1+y,3/2-z$; (v) $1+x,1-y,-1/2+z$.

	Commensurate *t* sections	
	0.25	0.75
V1-O1	1.651(2)	1.643(2)
V1-O9$^{(i)}$	1.737(2)	1.733(2)
V1-O12$^{(ii)}$	1.744(3)	1.732(3)
V1-O13$^{(ii)}$	1.733(3)	1.747(3)
V2-O2	1.644(2)	1.651(2)
V2-O8	1.8510(1)	1.8468(1)
V2-O10$^{(i)}$	1.716(2)	1.721(2)
V2-O11$^{(ii)}$	1.724(2)	1.714(2)
V3-O3	1.620(2)	1.616(2)
V3-O10$^{(ii)}$	2.036(2)	2.035(2)
V3-O15$^{(ii)}$	1.934(3)	1.938(3)
V3-O16$^{(ii)}$	1.932(3)	1.935(3)
V3-O16$^{(iii)}$	1.977(2)	1.968(2)
V4-O4	1.622(2)	1.615(2)
V4-O12$^{(ii)}$	1.953(2)	1.955(2)
V4-O13$^{(iv)}$	1.941(3)	1.923(3)
V4-O14$^{(ii)}$	1.953(3)	1.947(3)
V4-O18$^{(iv)}$	1.957(2)	1.988(2)
V5-O5	1.614(2)	1.606(2)
V5-O9$^{(ii)}$	1.971(2)	1.968(2)
V5-O15$^{(iii)}$	1.980(2)	1.985(2)
V5-O16$^{(ii)}$	1.949(3)	1.934(3)
V5-O17$^{(ii)}$	1.943(3)	1.975(3)
V6-O6	1.617(2)	1.621(2)
V6-O11$^{(ii)}$	2.014(2)	2.030(2)
V6-O14$^{(ii)}$	1.923(3)	1.927(3)
V6-O15$^{(ii)}$	1.929(3)	1.931(3)
V6-O17$^{(iii)}$	1.991(2)	1.979(2)
V7-O7	1.598(2)	1.594(2)
V7-O14$^{(iii)}$	1.939(2)	1.947(2)
V7-O17$^{(ii)}$	1.940(3)	1.877(3)
V7-O18$^{(i)}$	1.955(2)	1.814(2)
V7-O18$^{(v)}$	2.018(3)	1.907(3)

Additional information on the magnetic properties of $Na_9V_{14}O_{35}$ comes from the ESR data. Indeed, the ESR technique, being a local probe, allows us, along with other advantages, to distinguish between the signals of different magnetic species present in the sample. Figure 8 shows a series of *X*-band spectra taken between 10 K and 320 K on a single crystal of $Na_9V_{14}O_{35}$, the static magnetic field, **H**, being applied in the direction perpendicular to the (x,z) plane of the structure.

Two aspects may be noted in this series of spectra: the general trend followed by the ESR intensity while the temperature is lowered (a gradual increase followed by a more rapid decrease), and the appearance, at low temperature, of an additional signal, different from the main one. We attribute this additional signal to the impurities present in the sample and which we mentioned above. The spin susceptibility deduced from the ESR data by double integration of the ESR signal is shown in Fig. 9. The similarity between this curve and that shown in Fig. 7 confirms that the corrected susceptibility shown in Fig. 7 can be wholly attributed to the V^{4+} ions of $Na_9V_{14}O_{35}$. Furthermore, the room-temperature *g*-factor values, $g_\perp = 1.931$ and $g_\parallel = 1.973$, deduced from the ESR data for **H** perpendicular and **H** parallel to the (x,z) plane, respectively, are typical of V^{4+} ions in a fivefold pyramidal environment (see, e.g., Choukroun *et al.*[28] and Pashchenko *et al.*[29]).

TABLE V. Bond-valence-sum analysis for V atoms of $Na_9V_{14}O_{35}$ at 40 K. (V^{4+}, $r_0 = 1.784$ Å ; V^{5+}, $r_0 = 1.803$ Å.) The bold numbers underline the valence state (V^{4+} or V^{5+}) attributed to each vanadium site according to the bond-valence sum analysis.

	Commensurate *t* sections			
	0.25		0.75	
	V^{4+}	V^{5+}	V^{4+}	V^{5+}
V1	4.83	**5.08**	4.86	**5.12**
V2	4.67	**4.91**	4.67	**4.92**
V3	**3.99**	4.20	**4.01**	4.23
V4	**4.09**	4.31	**4.12**	4.33
V5	**4.06**	4.28	**4.07**	4.28
V6	**4.04**	4.25	**4.01**	4.22
V7	**4.13**	4.35	4.73	**4.98**

In order to try to understand the origin of the spin gap in this system, we first tried to fit the low-temperature part of the susceptibility curve by the law $\chi = A(1/T)^\alpha \exp(-\Delta/T)$ (inset of Fig. 7), with $\alpha = \frac{1}{2}$ (solid line) and $\alpha = 0$ (dashed line), the values appropriate for 1D and 2D systems,[30] respectively. The resulting values of Δ came out to be 35 ± 1 K for $\alpha = \frac{1}{2}$ and 29 ± 1 K for $\alpha = 0$. For the high-temperature part, we considered the simulations of the susceptibility of an *n*-spin ring (with *n* even) of antiferromagnetically coupled spin-$\frac{1}{2}$ ions (see, e.g., Bonner and Fisher[31]) with $J/k = 195$ K. The simulation of the complete curve (not shown here in order not to overload the figure), obtained with the association of this value of J/k and the gap value obtained for $\alpha = \frac{1}{2}$, corresponds to a number of spins $n = 22$. Considering that the magnetic unit cell in the low-temperature phase of $Na_9V_{14}O_{35}$ contains 18 spins, this result indicates that the exchange coupling between spins cannot have a unique value as would be the case in a ring.

The opening of the spin gap at low temperature is an independent proof that there must be charge ordering. Indeed, a general requirement for the occurrence of a magnetization plateau, originally derived by Oshikawa *et al.*[32] in 1D and generalized by Oshikawa[33] in any dimension is that $Sn(1-m)$ should be an integer, where *S* is the spin (here $\frac{1}{2}$), *n* the number of spins per unit cell of the magnetic model, and *m* is the ratio of the magnetization to the saturation value in the plateau. A spin gap is a special case with $m = 0$. Hence, for spin $\frac{1}{2}$, a spin gap can only occur if the number of magnetic sites per unit cell is even. In the high-temperature phase of $Na_9V_{14}O_{35}$, all finite-length ladders are magnetically equivalent, and there are effectively 9 spins per unit cell of the magnetic model. Hence the system cannot be gapped, contrary to the claim made by Whangbo and Koo[13] regarding the fused chain of 10-node rings. In the low-temperature phase however, according to the present study, there is a

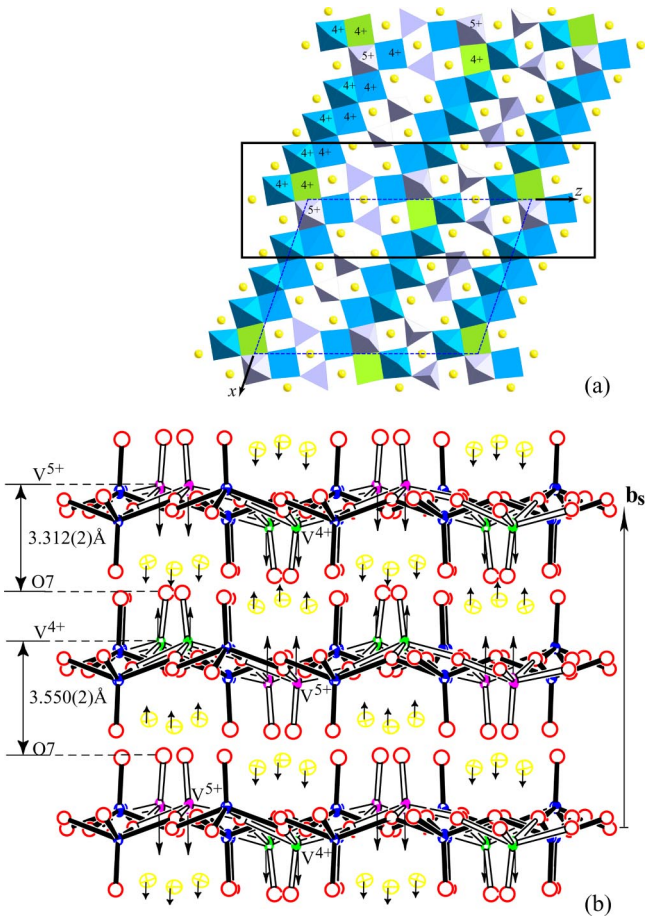

FIG. 5. (Color online) (a) Projection of the $T=40$ K $Na_9V_{14}O_{35}$ structure onto (010) below the transition. The oxidation state (4+ or 5+) of each vanadium atom along the double strings is indicated. (b) View normal to the [001] direction of the area surrounded in (a). This projection is represented in the supercell ($b_s=2b$). The displacements of the V7 atoms are indicated by arrows. The displacements in phase of the apical oxygen O7 are not represented for clarity. In order to distinguish V7-O polyhedra from the other V-O polyhedra, open bonds have been used for V7-O bonds. Large ellipsoïds between the layers represent Na1 and Na5 atoms, circles represent O atoms. The displacements of the Na1 and Na5 atoms are represented by small arrows.

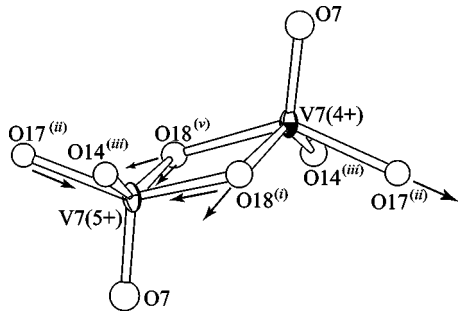

FIG. 6. Adjacent pyramids containing the V7 atoms. The arrows indicate the contraction and the expansion of those pyramids with respect to room temperature. The V7-V7 direction is along the **b** axis. Symmetry symbols as in Table IV.

TABLE VI. Bond lengths (Å) for Na-O polyhedra at 40 K. Symmetry codes: (vi) $-x,y,3/2-z$; (vii) $1-x,y,3/2-z$.

	Commensurate t sections	
	0.25	0.75
Na1-O1	2.354(2)	2.361(2)
Na1-O1$^{(vi)}$	2.354(2)	2.361(2)
Na1-O4	2.605(3)	2.634(3)
Na1-O4$^{(vi)}$	2.604(3)	2.634(3)
Na1-O12	2.959(3)	2.916(3)
Na1-O12$^{(vi)}$	2.959(3)	2.916(3)
Na1-O13	2.348(3)	2.354(3)
Na1-O13$^{(vi)}$	2.348(3)	2.354(3)
Na2-O2	2.330(2)	2.325(2)
Na2-O4	2.470(3)	2.467(3)
Na2-O6	2.425(3)	2.426(3)
Na2-O11	2.571(3)	2.572(3)
Na2-O12	2.356(3)	2.335(3)
Na2-O14	2.396(3)	2.407(3)
Na3-O3	2.378(3)	2.349(3)
Na3-O6	2.347(3)	2.347(3)
Na3-O8	2.477(2)	2.473(2)
Na3-O10	2.412(3)	2.436(3)
Na3-O11	2.440(3)	2.433(3)
Na3-O15	2.335(3)	2.348(3)
Na4-O2$^{(vii)}$	2.388(3)	2.394(3)
Na4-O3	2.440(3)	2.441(3)
Na4-O5	2.387(3)	2.402(3)
Na4-O9	2.391(3)	2.370(3)
Na4-O10	2.550(3)	2.544(3)
Na4-O16	2.409(3)	2.401(3)
Na5-O1$^{(vii)}$	2.450(3)	2.479(3)
Na5-O4	3.066(2)	3.069(2)
Na5-O5	2.565(2)	2.599(3)
Na5-O7	2.315(3)	2.357(3)
Na5-O9	2.526(3)	2.551(3)
Na5-O13$^{(vii)}$	2.521(2)	2.502(2)
Na5-O17	2.455(3)	2.393(3)
Na5-O18$^{(vii)}$	2.600(3)	2.586(3)

doubling of the unit cell of the magnetic model due to charge ordering, and there are now 18 spins per unit cell. In this respect, the magnetic properties are consistent with the structural determination of the low-temperature phase.

Beyond this qualitative statement, the precise mechanism of the gap opening will depend strongly on the value of the exchange integrals. Given the rather large number of nonequivalent bonds, it is not possible at the moment to make a reliable proposal. We just note, however, that the gap opening has to be due to some residual coupling beyond nearest- and next-nearest-neighbor couplings between $V^{4+}O_5$ pyramids, because, with the structural distortion and charge localization reported here, the effective model would otherwise consist of decoupled chains with 9 spins per unit cell (see Fig. 10). This remark is consistent with the fact that the gap is significantly smaller than the dominant couplings in the system. A detailed analysis of this problem will be reported elsewhere.

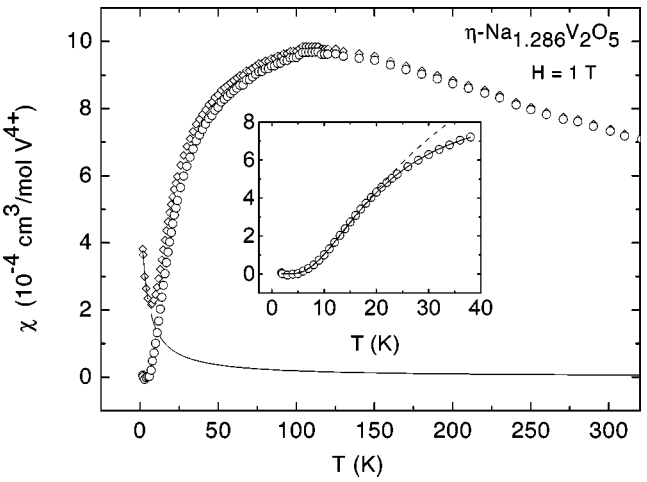

FIG. 7. The temperature dependence of the magnetic susceptibility of $Na_9V_{14}O_{35}$ under a magnetic field $H=1$ T. Open diamonds represent the raw data, χ_{raw}; the solid line represents the impurity contribution, χ_{imp}; open circles represent the corrected susceptibility, χ, defined as $\chi=\chi_{raw}-\chi_{imp}$. The inset shows an enlarged view of the low-temperature corrected susceptibility, fitted with the law $\chi=A(1/T)^{\alpha}\exp(-\Delta/T)$, with $\alpha=\frac{1}{2}$ (solid line) and $\alpha=0$ (dashed line), the corresponding values of Δ being 35 ± 1 K and 29 ± 1 K, respectively.

V. CONCLUSION

With the help of low-temperature x-ray diffraction measurements performed on single crystals of $Na_9V_{14}O_{35}$, we have given evidence for the existence, around 100 K, of a structural second-order phase transition in this compound, resulting in the doubling of the unit cell in the **b** direction. We have also shown that the superstructure formation is associated with an alternating charge ordering on the V7 sites. Moreover, diffusion scattering measurements give evidence that the Coulomb repulsions are responsible for this transition. The Na atoms, which ensure the balance of charges, are sensitive to this charge ordering. On the other hand, the magnetic measurements are consistent with the structural and charge ordering transition, particularly by showing the opening of a spin gap, which we have discussed in association with the doubling of the magnetic unit cell. Further studies are now needed in order to precisely determine the exchange integrals between the various magnetic sites.

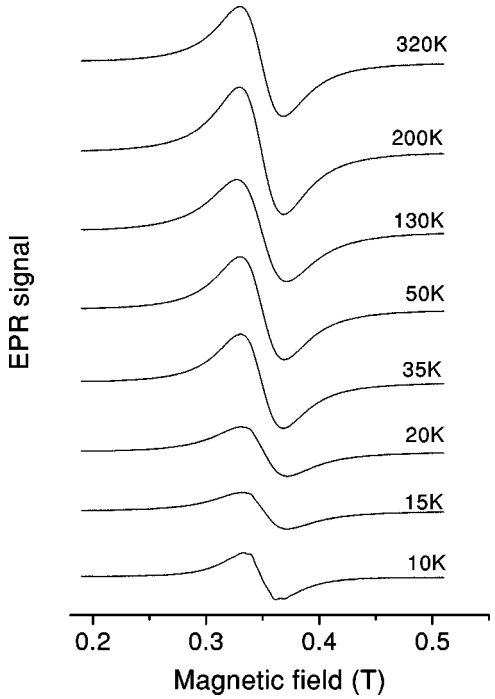

FIG. 8. A series of ESR spectra of $Na_9V_{14}O_{35}$ taken in the X band ($\nu=9.635$ GHz) at various temperatures between 10 K and 320 K, the static magnetic field being perpendicular to the (x,z) plane of the structure. The appearance of an additional signal at low temperature is attributed to impurities.

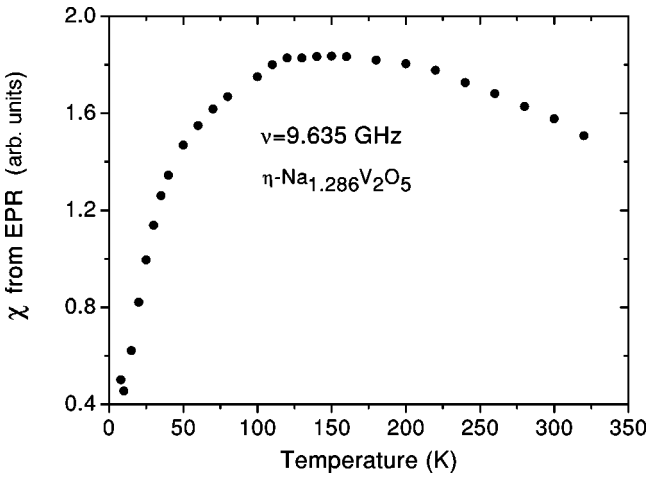

FIG. 9. The temperature dependence of the susceptibility of $Na_9V_{14}O_{35}$ as deduced from the ESR spectra by double integration of the ESR signal.

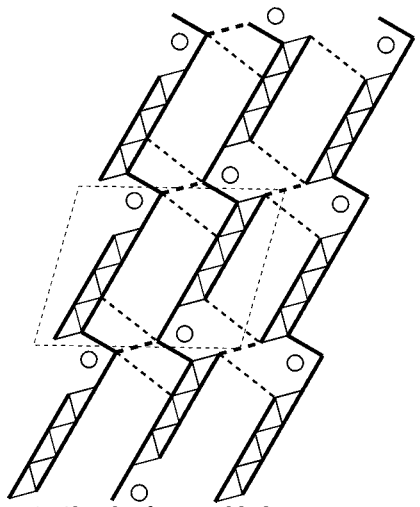

FIG. 10. Sketch of a possible low-temperature magnetic model. The very thin dashed line is the unit cell. The vanadium atoms in the oxidation state V^{5+} in the double string are represented by circles. The solid lines are the intraladder couplings, and the dashed lines are the interladder couplings. Without these interladder couplings, the system would be a collection of decoupled, gapless chains.

ACKNOWLEDGMENTS

We thank David Warner from Oxford Diffraction for his technical assistance with the Helijet open flow helium cooler. Two of the authors (F.D. and P.M.) are grateful to Bruno Donnadieu and Jean-Claude Daran from the Laboratoire de Chimie de Coordination (UPR CNRS 8241, Toulouse) for making the Xcalibur CCD diffractometer available to them. We also thank V. A. Pashchenko and J.-Y. Henry for their help in the magnetic measurements and for stimulating discussions.

*Electronic address: fduc@cemes.fr

[1] M. Azuma, Z. Hiroi, M. Takano, K. Ishida, and Y. Kitaoka, Phys. Rev. Lett. **73**, 3463 (1994).

[2] M. Isobe, T. Ohta, M. Onoda, F. Izumi, S. Nakano, J. Q. Li, Y. Matsui, E. Takayama-Muromachi, T. Matsumoto, and H. Hayakawa, Phys. Rev. B **57**, 613 (1998).

[3] E. Dagotto and T.M. Rice, Science **271**, 618 (1996).

[4] M. Isobe and Y. Ueda, J. Phys. Soc. Jpn. **65**, 1178 (1996).

[5] Y. Tokura, Y. Taguchi, Y. Okada, Y. Fujishima, T. Arima, K. Kumagai, and Y. Iye, Phys. Rev. Lett. **70**, 2126 (1993); B. Keimer, D. Casa, A. Ivanov, J. W. Lynn, M. v. Zimmermann, J. P. Hill, D. Gibbs, Y. Taguchi, and Y. Tokura, *ibid.* **85**, 3946 (2000)

[6] H. Smolinski, C. Gros, W. Weber, U. Peuchert, G. Roth, M. Weiden, and C. Geibel, Phys. Rev. Lett. **80**, 5164 (1998).

[7] T. Ohama, H. Yasuoka, M. Isobe, and Y. Ueda, Phys. Rev. B **59**, 3299 (1999).

[8] J. Lüdecke, A. Jobst, S. vanSmaalen, E. Morr, C. Geibel, and H.-G. Krane, Phys. Rev. Lett. **82**, 3633 (1999); J.L. de Boer, SA. Meetsma, J. Baas, and T.T.M. Palstra, *ibid.* **84**, 3962 (2000).

[9] S. Grenier, A. Toader, J. E. Lorenzo, Y. Joly, B. Grenier, S. Ravy, L. P. Regnault, H. Renevier, J. Y. Henry, J. Jegoudez, and A. Revcolevschi, Phys. Rev. B **65**, 180101 (2002).

[10] N. Suaud and M.B. Lepetit, Phys. Rev. Lett. **88**, 56 405 (2002).

[11] P. Millet, J.-Y. Henry, and J. Galy, Acta Crystallogr., Sect. C: Cryst. Struct. Commun. **C55**, 276 (1999).

[12] M. Isobe, Y. Ueda, Y. Oka, and T. Yao, J. Solid State Chem. **145**, 361 (1999).

[13] M.-H. Whangbo and H.-J Koo, Solid State Commun. **115**, 115 (2000).

[14] J.-Y. Henry (private communication).

[15] Although charge-ordering transitions in manganites are strongly first order, suggesting it is an intrisic feature of charge ordering, continuous charge-ordering transitions have been already observed in organic systems—see, e.g., D. S. Chow, F. Zamborszky, B. Alavi, D. J. Tantillo, A. Baur, C. A. Merlic, and S. E. Brown, Phys. Rev. Lett. **85**, 1698 (2000).

[16] See EPAPS Document No. E-PRBMDO-69-036401 for supplementary data at 15 K. A direct link to this document may be found in the online article's HTML reference section. The document may also be reached via the EPAPS homepage (http://www.aip.org/pubservs/epaps.html) or from ftp.aip.org in the directory /epaps/. See the EPAPS homepage for more information.

[17] XcaliburSystem, User Manual. Crysalis Software Package, version 1.167 (Oxford Diffraction, Oxfordshire, U.K., 2001).

[18] P.M. de Wolff, Acta Crystallogr., Sect. A: Cryst. Phys., Diffr., Theor. Gen. Crystallogr. **A30**, 777 (1974).

[19] T. Janssen, A. Janner, A. Looijenga-Vos, and P. M. de Wolff, *International Tables for Crystallography*, Vol. C, *Mathematical, Physical and Chemical Tables*, edited by A.J.C. Wilson (Kluwer Academic Publishers, Dordrecht, Boston, London, 1992).

[20] A. Schönleber, M. Meyer, and G. Chapuis, J. Appl. Crystallogr. **34**, 777 (2001).

[21] M. Dušek (private communication).

[22] A. Yamamoto, Acta Crystallogr., Sect. A: Found. Crystallogr. **A52**, 509 (1996).

[23] V. Petříček and M. Dušek, JANA2000, Structure Determination Software Programs (Institute of Physics, Praha, Czech Republic, 2000).

[24] The atomic positions x_i^μ in a one-dimensionally modulated structure are given as the sum of an average position and a shift: $x_i^\mu = \bar{x}_i^\mu + u_i^\mu(\bar{x}_4)$, $\bar{x}_i^\mu = L_i + \bar{x}_i^{0\mu}$, $\bar{x}_4 = t_0 + \mathbf{q}\cdot\mathbf{x}$, where $\bar{x}_i^\mu$ $(i=x,y,z)$ are the coordinates of an atom μ in the average structure, L_i are integers, and $\bar{x}_i^{0\mu}$ the average position within the unit cell. The components of the modulation function of atom μ are $u_i^\mu(\bar{x}_4)$ with $u_i^\mu(\bar{x}_4+1) = u_i^\mu(\bar{x}_4)$. $\bar{x}_4 = t_0 + \mathbf{q}\cdot\mathbf{x}$ is the fourth superspace coordinate with starting phase t_0. $u_i^\mu(\bar{x}_4) = A_i \sin(2\pi\bar{x}_4) + B_i \cos(2\pi\bar{x}_4)$.

[25] A. Janner and T. Janssen, Physica A **99**, 47 (1979).

[26] The superspace is defined as $(D+d)$-dimensional Euclidean vector space with two distinguishable subspaces: the D-dimensional space V_E and the d-dimensional space V_I. By this way one can define the superspace V_S as an Euclidean metric (Ref. 25) $V_S = V_E \oplus V_I$. The subspace V_E is identified with the physical space **R**. It is called external, physical, parallel, or position space (V_E or $V_\parallel$). The additional dimension(s) are called internal, complementary, or perpendicular space (V_I or $V_\perp$). Because of the Euclidean metric V_I is orthogonal to V_E.

[27] D. Brown and D. Altermatt, Acta Crystallogr., Sect. B: Struct. Sci. **B41**, 244 (1985).

[28] J. Choukroun, V.A. Pashchenko, Y. Ksari, J.Y. Henry, F. Mila, P. Millet, P. Monod, A. Stepanov, J. Dumas, and R. Buder, Eur. Phys. J. B **14**, 655 (2000).

[29] V.A. Pashchenko, A. Sulpice, F. Mila, P. Millet, A. Stepanov, and P. Wyder, Eur. Phys. J. B **21**, 473 (2001).

[30] S. Taniguchi, T. Nishikawa, Y. Yasui, Y. Kobayashi, M. Sato, T. Nishioka, M. Kontani, and K. Sano, J. Phys. Soc. Jpn. **64**, 2758 (1995).

[31] J. C. Bonner and M. E. Fisher, Phys. Rev. **135**, A640 (1964).

[32] M. Oshikawa, M. Yamanaka, and I. Affleck, Phys. Rev. Lett. **78**, 1984 (1997).

[33] M. Oshikawa, Phys. Rev. Lett. **84**, 1535 (2000).

[34] P.J. Becker and P. Coppens, Acta Crystallogr., Sect. A: Cryst. Phys., Diffr., Theor. Gen. Crystallogr. **A30**, 129 (1974).